J Mater Sci (2007) 42:1455–1465
DOI 10.1007/s10853-006-0670-y

Grain size dependence of strength of nanocrystalline materials as exemplified by copper: an elastic-viscoplastic modelling approach

S. Mercier · A. Molinari · Y. Estrin

Received: 8 April 2006 / Accepted: 13 July 2006 / Published online: 4 January 2007

Abstract The purpose of this work is to model the mechanical behavior of nanocrystalline materials. Based on previous rigid viscoplastic models proposed by Kim et al. (Acta Mater, 48: 493, 2000) and Kim and Estrin (Acta Mater, 53: 765, 2005), the nanocrystalline material is described as a two phase composite material. Using the Taylor–Lin homogenisation scheme in order to account for elasticity, the yield stress of nanocrystalline materials can be evaluated. The transition from a Hall–Petch relation to an inverse Hall–Petch relation is defined and is related to a change in plastic deformation mode in the crystallite phase from a dislocation glide driven mechanism to a diffusion-controlled process.

Introduction

With the advent of nanostructured materials, there has been a growing interest—both in the materials science and in the mechanics communities—in reliable constitutive models describing the mechanical response of bulk nanomaterials. Obviously, by the very nature of the problem, internal structure associated with ultra fine crystallinity of the material, as well as grain boundary effects, need to figure prominently in such a model, one particular requirement being an adequate description of the grain size effects. The experimental literature on the grain size dependent mechanical properties of nanocrystalline materials and the existing modelling approaches to their behaviour are summarised in an excellent review by Meyers et al. [1].

In a nanocrystalline material, whose grain size d by a common definition is smaller than 100 nm, the grain boundaries make up a significant volume fraction of the material. As the constitutive behaviour of the grain boundary regions and the grain interior are radically different, cf. [1], it is a natural thought to consider a nanocrystalline material as a 'phase mixture' and apply a rule of mixtures as a modelling tool. Such approach was taken in the work by [2–7].

The phase mixture model proposed by Kim et al. [2] and Kim and Estrin [3] (see also Estrin et al. [7]) was based on a combination of dislocation glide diffusion controlled mechanisms for grain interior deformation and purely diffusional flow of the grain boundary phase. The model was shown to capture the most significant features of strength and plasticity of nanocrystalline materials, such as the breakdown of the Hall–Petch relation for very small grain sizes, and to adequately represent their strain hardening behaviour. However, some quantitative discrepancies between the model predictions and the experimental data for copper were found. While these discrepancies may be partly associated with the 'inborn' flaws of the test material inherent in the processing techniques used, we

S. Mercier (✉) · A. Molinari
Laboratory of Physics and Mechanics of Materials, UMR CNRS 7554, Université Paul Verlaine-Metz, Ile du Saulcy 57045 Metz, France
e-mail: sebastien.mercier@univ-metz.fr

A. Molinari
e-mail: alain.molinari@univ-metz.fr

Y. Estrin
Institute of Materials Science and Technology, Clausthal University of Technology, Agricolastr. 6, 38678 Clausthal-Zellerfeld, Germany
e-mail: juri.estrin@tu-clausthal.de

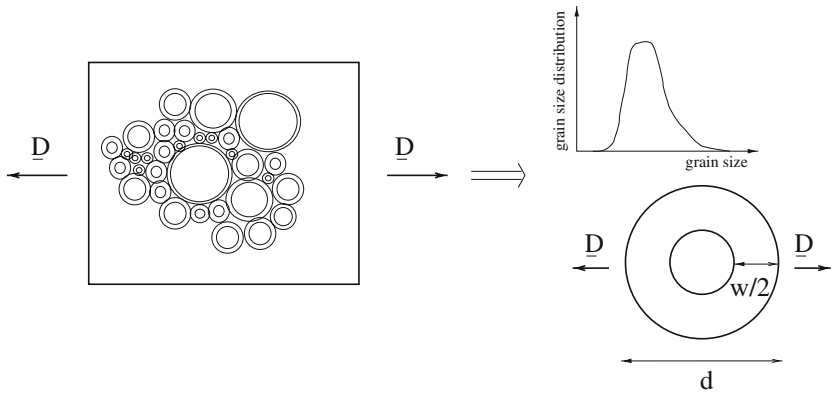

Fig. 1 Schematic representation of a nanocrystalline material. The crystallite phase is embedded in the grain boundary phase. The grain size distribution in the material is represented by Eq. 1. Each grain is assumed to be subjected to the macroscopic strain rate. A Taylor–Lin scheme is adopted to derive the macroscopic behavior of the aggregate

now believe that part of the problem was that elasticity was disregarded. Also, the topology of the grain and grain boundary structure was not accounted for.

Since a nanomaterial can be described as a two phase material, different homogenization schemes can be used to describe the material response of such material. Capolungo et al. [8, 9] used a self-consistent scheme representing the interior of a grain as an ellipsoidal Eshelby-type inclusion and also modified the description of the grain boundary deformation. Jiang and Weng [10] have proposed a generalized self-consitent approach based on the Christensen and Lo's [11] and Luo and Weng's [12] works. The plastic behaviour of the grain interior phase is described by crystal plasticity and the grain boundary phase is considered as an amorphous material. Instead of adopting a self-consistent scheme, we propose to use the Taylor–Lin approach to include elasticity [13], in conjunction with the original model due to [2, 3]. The present authors have tested also an extension of the Mori–Tanaka approach [14] based on an interaction law proposed by Molinari [15] for elastic-viscoplastic materials. Since the volume fraction of grain boundary remains limited (at least for nanocrystalline materials with average grain size over 20 nm), the Taylor–Lin and the Mori–Tanaka approaches provide similar results so that only results obtained via the Taylor–Lin scheme are reported in the present contribution.

While in considering the case of strain rate independent rigid plasticity Taylor [16] assumed that each grain is subjected to the same uniform *plastic strain* in all grains of a polycrystal, Lin [13] extended Taylor's model to include *elastic strains* as well. In the Taylor–Lin scheme, the total deformation (elastic plus plastic) in each grain is equal to the imposed total deformation of the polycrystalline aggregate. This model has been used extensively to predict the development of textures in polycrystals under monotonic loadings [17, 18], the cyclic behavior of polycrystalline metals [19, 20] and the low cycle fatigue response of materials [21, 22]. Since the main goal of the present work is to predict the yield stress of nanocrystalline materials, the interplay between the elastic and viscoplastic response of the constituents of the 'phase mixture' needs to be taken into account. The Taylor–Lin scheme provides a suitable frame for that. It will be shown that the use of the Taylor–Lin scheme in conjunction with the original model [2, 3] does possess an improved predictive capability and can be recommended for describing the mechanical behaviour of bulk nanocrystalline materials.

Modelling

Following the model by [2, 3], a nanocrystalline material is described as a two phase composite material. A crystallite (the grain interior) is considered to be embedded in the grain boundary phase. Both phases (crystallite and grain boundary) are assumed to be homogeneous. From a topological point of view, the crystallite can be considered as the inclusion phase and the grain boundary as the matrix phase. Nevertheless, the volume fraction of grain boundary (the matrix phase) is limited. For nanocrystalline materials with an average grain size of 10 nm, the matrix phase is about 30%. The macroscopic nanocrystalline material is described as an aggregate of spherical grains, with different grain sizes. A log-normal distribution of the grain sizes is assumed, cf. Fig. 1 that gives a schematic representation of the aggregate. Some measurements available in the literature [23–25] do corroborate this type of distribution. The distribution of grain diameter d is governed by the probability density function:

$$P(d) = \frac{1}{(2\pi)^{\frac{1}{2}}\sigma d}\exp\left(-\frac{1}{2}\left(\frac{\ln(d/d_{\mathrm{o}})}{\sigma}\right)^2\right) \qquad (1)$$

where d_o and σ are constant parameters. The mean size $\bar{d}$ and the variance $\tilde{\sigma}$, quantities that can be obtained from experiment, are linked to d_o and σ through the following relations:

$$\bar{d} = d_o \exp(\frac{1}{2}\sigma^2) \quad \tilde{\sigma} = d_o^2 \exp(\sigma^2)(\exp(\sigma^2) - 1) \tag{2}$$

A Taylor–Lin scheme is adopted for deriving the macroscopic behavior of the nanocrystalline material, implying that each grain is subjected to the same strain rate tensor, equal to the macroscopic tensor $\underline{D}$, see Fig. 1. Owing to this assumption, the topology of the grain and grain boundary structure is not accounted for except through the volume fraction of grain interior phase. A Mori–Tanaka scheme would have been able to describe the topology of a nanomaterial in a better way. Nevertheless, as mentioned in the previous section, results within the Mori–Tanaka approach were similar so that only the Taylor–Lin approach is developed in the present contribution.

Both phases of the grain are considered to exhibit elastic-viscoplastic behaviour. Incompressible elasticity is assumed. The general case of compressible elasticity can be easily treated with the Taylor–Lin approach by decomposition of the deviatoric and spherical parts of the stress and strain-rate tensors. In the Taylor–Lin approach, deviatoric and spherical parts can be decoupled for isotropic materials. Only the hydrostatic pressure will be affected by the elastic compressibility.

The model of plastic flow of a nanocrystalline material developed by [2, 3] is briefly summarised below, in the context of the Taylor–Lin formulation, i.e. including elasticity. For the grain boundary phase, the elastic contribution is described by the following law:

$$\dot{\underline{s}}_{GB} = 2\mu_{GB}(\underline{d}_{GB} - \underline{d}^{vp}_{GB}) \tag{3}$$

where $\underline{d}_{GB}$ and $\underline{d}^{vp}_{GB}$ are the tensors of the total and the viscoplastic strain rate, respectively. As prescribed by the Taylor–Lin assumption, $\underline{d}_{GB} = \underline{D}$. The rate of the deviatoric Cauchy stress tensor has been denoted $\dot{\underline{s}}_{GB}$, the shear modulus μ_{GB} of the grain boundary material has been introduced. Using a J_2 flow theory, the viscoplastic behaviour of the grain boundary, governed by diffusional mechanism, see [2], is expressed by the Prandtl–Reuss equation:

$$\underline{s}_{GB} = \frac{2}{3}\frac{\sigma^{eq}_{GB}}{d^{eq}_{GB}}\underline{d}^{vp}_{GB} \tag{4}$$

with

$$d^{eq}_{GB} = D^{sd}_{bd}\frac{\Omega_b}{kT}\frac{2d - w}{d^3}\sigma^{eq}_{GB} \tag{5}$$

Here $\underline{s}_{GB}$ stands for the deviatoric Cauchy stress tensor. $d^{eq}_{GB} = \sqrt{\frac{2}{3}\underline{d}^{vp}_{GB} : \underline{d}^{vp}_{GB}}$ denotes the (von Mises) equivalent strain rate and $\sigma^{eq}_{GB} = \sqrt{\frac{3}{2}\underline{s}_{GB} : \underline{s}_{GB}}$ the equivalent stress in the grain boundary. Ω_b is the atomic volume, D^{sd}_{bd} the grain boundary diffusivity, k the Boltzmann constant and T the absolute temperature. The grain boundary thickness w was assumed to be constant, regardless of the grain size, $w = 1$ nm being a generally accepted value.

Whereas the deformation mechanism in the grain boundary phase was modelled as a purely diffusion-controlled one, that of the grain interior was considered to be comprised by three contributions to the plastic flow operating in parallel, namely the dislocation glide mechanism, the Coble creep and the Nabarro–Herring creep.

Similarly to the grain boundary phase, the crystalline phase is described by the following equation:

$$\dot{\underline{s}}_{GI} = 2\mu_{GI}(\underline{d}_{GI} - \underline{d}^{vp}_{GI}) \tag{6}$$

where the subscript GI refers to quantities relating to the grain interior (crystallite). As for the grain boundary phase, the viscoplastic behavior of the crystallite follows a J_2 flow law, similar to Eq. 4. The total plastic strain rate tensor, $\underline{d}^{vp}_{GI}$, for the grain interior is assumed to be made up by three additive contributions:

$$\underline{d}^{vp}_{GI} = \underline{d}^{disl}_{GI} + \underline{d}^{Co}_{GI} + \underline{d}^{NH}_{GI} \tag{7}$$

where $\underline{d}^{disl}_{GI}$ represents the plastic strain rate tensor due to dislocation activity, $\underline{d}^{Co}_{GI}$ is the corresponding tensor associated with the Coble creep and $\underline{d}^{NH}_{GI}$ that for the Nabarro–Herring creep.

To describe the dislocation contribution to the deformation of the grain interior, a dislocation density related unified constitutive model [25] is used. The equivalent plastic strain rate due to dislocation glide $d^{disl-eq}_{GI}$ is expressed in terms of the equivalent stress in the grain interior, σ^{eq}_{GI}, through a power-law:

$$d^{disl-eq}_{GI} = d_*\left(\frac{\sigma^{eq}_{GI}}{\sigma_o}\right)^m\left(\frac{\rho}{\rho_o}\right)^{-\frac{m}{2}} \tag{8}$$

where $1/m$ represents the strain rate sensitivity of the flow stress. d_* and σ_o are scaling parameters and ρ is the dislocation density with the initial value ρ_o. The evolution law for the dislocation density is written as in [2]:

$$\frac{\mathrm{d}\rho}{\mathrm{d}t} = d_{GI}^{\mathrm{disl-eq}}\rho_{\mathrm{o}}\left(C + C_1\sqrt{\frac{\rho}{\rho_{\mathrm{o}}}} - C_2\left(\frac{d_{\mathrm{GI}}^{\mathrm{disl-eq}}}{d_1}\right)^{-\frac{1}{n}}\frac{\rho}{\rho_{\mathrm{o}}}\right) \tag{9}$$

It accounts for storage and concurrent annihilation of dislocations. Here C, C_1, C_2, d_1 and n are constants. Representative values for pure copper are available in the literature and are summarized in Table 1. The quantity C accounts for the dislocation storage associated with impermeable grain boundaries and is inversely proportional to the average grain size [2]:

$$C = \frac{Mb}{\bar{d}}\left(\frac{M\alpha\mu_{GI}}{\sigma_{\mathrm{o}}}\right)^2 \tag{10}$$

Here b is the Burgers vector, M the Taylor factor and α a numerical constant. For coarse-grained, single-phase materials, C can be set to zero.

The equivalent plastic strain rate associated with lattice diffusion follows the classical Nabarro–Herring relation:

$$d_{\mathrm{GI}}^{\mathrm{NH-eq}} = 14\frac{\Omega_b D_{\mathrm{ld}}^{\mathrm{sd}} w}{kTd^2}\sigma_{\mathrm{GI}}^{\mathrm{eq}} \tag{11}$$

where $D_{\mathrm{ld}}^{\mathrm{sd}}$ represents the lattice diffusivity. Finally, the contribution due to the Coble mechanism is expressed as:

$$d_{\mathrm{GI}}^{\mathrm{Co-eq}} = 14\pi\frac{\Omega_b D_{\mathrm{bd}}^{\mathrm{sd}} w}{kTd^3}\sigma_{\mathrm{GI}}^{\mathrm{eq}} \tag{12}$$

To summarize, the proposed model is an extension of the Kim et al. [2] approach where elasticity has now been fully integrated. The macroscopic deviatoric stress $\underline{S}$ is derived as an average of the microscopic stress $\underline{s}$ over the volume V of the aggregate:

$$\underline{S} = \frac{1}{V}\int_V \underline{s}\mathrm{d}V \tag{13}$$

If all grains in the nanocrystalline material are of the same size, then Eq. 13 leads to:

$$\underline{S} = f\underline{s}_{\mathrm{GI}} + (1-f)\underline{s}_{\mathrm{GB}} \tag{14}$$

where $f = (d\text{–}w)^3/d^3$ is the volume fraction of the crystallite phase in a nanocrystalline grain.

Results

Macroscopic behavior of nanocrystalline copper

Experimental observations [23–26] have shown that grain sizes in a nanocrystalline material fluctuate strongly in the volume.To describe the scatter in size, the log-normal distribution law (1) is adopted. A discretization of the continuous distribution is proposed in the following. For a given mean grain size $\bar{d}$, the nanocrystalline material is described as an aggregate of N ($N >> 1$) families with the grain size in the interval $[0.15\bar{d} - 3.15\bar{d}]$. A uniform grain size from within this interval is attributed to each family. The density of grains for the i-th ($1 \le i \le N$) family, with the grain size $d_i = 0.15\bar{d} + \frac{3(2i-1)\bar{d}}{2N}$ ascribed to it, is given by:

$$\mathrm{Dens}(d_i) = \int_{d_i-\frac{3\bar{d}}{2N}}^{d_i+\frac{3\bar{d}}{2N}} P(x)\mathrm{d}x \tag{15}$$

Figure 2 presents the discretization scheme adopted in the calculations, with $N = 30$, $\bar{d} = 26\,\mathrm{nm}$ and for three different variance values. A larger variance leads to a broader distribution and therefore to a higher heterogeneity of grain sizes. It has been observed that the number of families involved in the discretization has little influence on the overall behavior when N is larger than 10. The effect of the variance on the macroscopic behavior is illustred in Fig. 3. The material is subjected to the following macroscopic strain rate corresponding to uniaxial tensile loading, for an isotropic incompressible material:

$$\underline{D} = D_{\mathrm{o}}\begin{bmatrix} 1 & 0 & 0 \\ 0 & -0.5 & 0 \\ 0 & 0 & -0.5 \end{bmatrix} \tag{16}$$

Note that D_{o} represents the equivalent macroscopic strain rate. Figure 3 shows predictions with regard to the macroscopic behavior of nanocrystalline copper

Table 1 Parameter values used in the calculations, see Kim et al. [2]

$D_{\mathrm{bd}}^{\mathrm{sd}} = 2.6 * 10^{-20}\mathrm{m}^2/\mathrm{s}$	$D_{\mathrm{ld}}^{\mathrm{sd}} = 1.51 * 10^{-40}\,\mathrm{m}^2/\mathrm{s}$	$\sigma_{\mathrm{o}} = 180$ MPa	$d_* = 0.005/\mathrm{s}$	$d_1 = 1/\mathrm{s}$
$m = 230$	$\mu_{\mathrm{GB}} = 25.26\,\mathrm{GPa}$	$\mu_{\mathrm{GI}} = 42.1\mathrm{GPa}$	$w = 1$ nm	$C_1 = 52.86$
$C_2 = 18.5$	$n = 21.2$	$b = 0.256$ nm	$M = 3.06$	$\alpha = 0.33$
$\Omega_b = 1.18 * 10^{-29}\,\mathrm{m}^3$	$k = 1.38\ *10^{-23}$ J/K	$T = 300$ K		

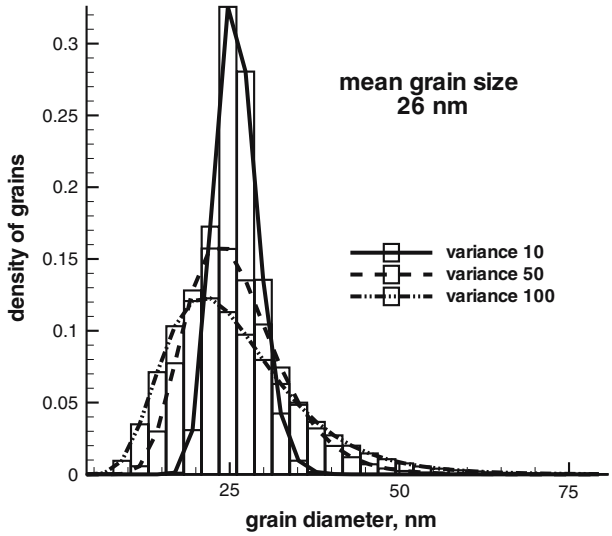

Fig. 2 Discretisation scheme adopted for the log-normal distribution law. The aggregate is made of 30 families. Each grain in a family has identical grain size. The density of grains in a family is given by Eq. 15 and is represented by the area in a vertical bin. In the present example, the average grain size is $\bar{d} = 26\,\text{nm}$ and three different values of the variance are adopted: $\tilde{\sigma} = 10, 50, 100\,\text{nm}^2$

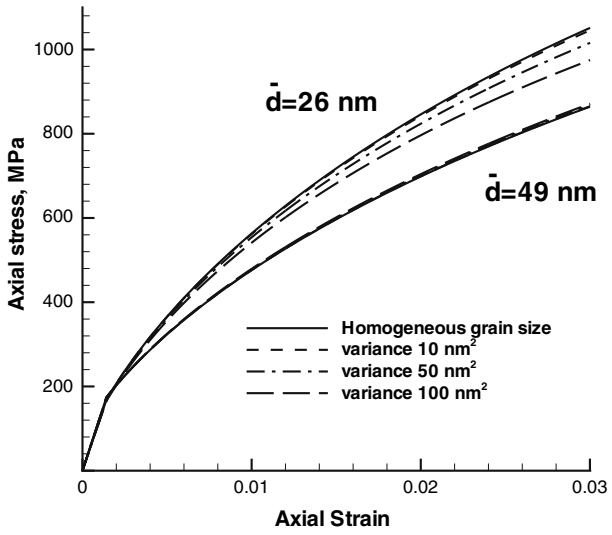

Fig. 3 Effect of the grain size distribution on the macroscopic behavior of the nanocrystalline copper, for different average grain sizes $\bar{d}$ and variances $\tilde{\sigma}$. Note the weak effect of $\tilde{\sigma}$ for large grain size

during uniaxial tensile loading with $D_o = 10^{-3}\,\text{s}^{-1}$. Materials with two different values of the mean grain size, $\bar{d} = 26\,\text{nm}$ and $\bar{d} = 49\,\text{nm}$, for which experimental data are available (shown in Fig. 4), were considered. The grain size distribution can strongly vary depending on the processing route used to produce the nanocrystalline material. To capture this

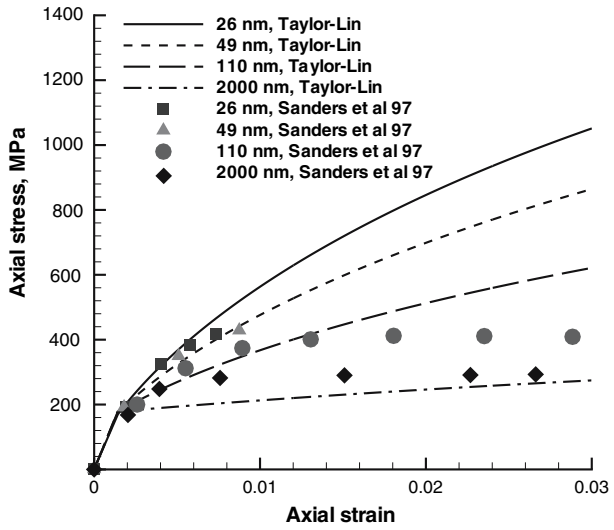

Fig. 4 Stress vs strain curves for copper. The grain size is varied from 26 to 2000 nm. The macroscopic strain rate corresponds to uniaxial tensile test, see Eq. 16 with $D_o = 10^{-3}\,\text{s}^{-1}$. The predictions based on the elastic-viscoplastic model are compared with the measurements by Sanders et al. [27]

effect, for a fixed mean grain size $\bar{d}$, the variance was varied ($\tilde{\sigma} = 10, 50, 100\,\text{nm}^2$). The predicted macroscopic behavior of the nanocrystalline material made up of grains of uniform size is also presented in this figure. For a nanocrystalline material with $\bar{d} = 26\,\text{nm}$, the grain size distribution has a significant influence on the stress-strain curves. Thus, a 7% difference in stress was observed at 0.03 total longitudinal strain when comparing the material with a broad grain size distribution ($\tilde{\sigma} = 100\,\text{nm}^2$) with that with a uniform grain size. For larger mean grain size, $\bar{d} = 49\,\text{nm}$, the effect of the distribution shape is negligible, as seen from the results of the simulation, cf. Fig. 3.

With this observation in mind, in the following, the effect of the grain size distribution will be disregarded, i.e. a nanocrystalline material will be considered to have uniform grain size. Since the macroscopic loading is given by relation (16) which corresponds to uniaxial tension, and since all grains have the same size, the macroscopic stress is given by Eq. 14. Accordingly, the equivalent macroscopic stress Σ^{eq}, which corresponds to the uniaxial tensile stress, is defined as, see Appendix B:

$$\Sigma^{\text{eq}} = f\sigma_{\text{GI}}^{\text{eq}} + (1-f)\sigma_{\text{GB}}^{\text{eq}} \tag{17}$$

Figure 4 presents stress–strain curves of nanocrystalline copper obtained using the proposed elastic-viscoplastic approach. The macroscopic strain rate corresponds to uniaxial tensile test, see Eq. 16 with

$D_o = 10^{-3}$ s^{-1}. The predictions are compared with the experimental results of Sanders et al. [27]. A reasonable agreement between simulations and experiments is observed for limited strain (below 0.01 total strain). The response at large strain is not accurately predicted for the nanomaterial having an average grain size of 110 nm. Since our attention is mainly focused on the grain size dependence of the yield stress, the proposed constitutive model appears to be adequate.

Hall–Petch and Inverse Hall–Petch behavior

Classically, the yield stress of materials increases with grain size refinement and follows a Hall–Petch relation. However, as the grain size enters the nanometer range, deviations from the Hall–Petch behaviour have often been observed. An inverse Hall–Petch behaviour, i.e. a decrease of the flow stress on further grain refinement has been reported, cf. [1, 28]. While there is still some debate on whether this anomaly is a genuine effect or an artefact associated with imperfections introduced by specimen preparation (van Swygenhoven and Weertman [29]), numerous models have been put forward to capture the inverse Hall–Petch behaviour (for recent discussions, see [1, 30, 31]). Kim et al. [2], neglecting elasticity, were able to predict this effect. However, some ad hoc assumptions, including the introduction of an artificial cut-off grain size for the dislocation activity and an assumed value of the yield stress of the grain boundary phase were necessary. Indeed, dislocation glide is difficult or impossible when the grain size is below about 8 nm in copper (cut-off value adopted by [2] for the dislocation activity). Besides, the mechanical behavior of the grain boundary phase is described by Eq. 5. As the grain size increases, the level of the flow stress reaches unreasonably large values. Accordingly, a saturation of the flow stress of the grain boundary phase on grain size increase was assumed by [2]. In addition, since elasticity was not included, Kim et al. [2] calculated the yield strength as the stress at 0.2% offset strain. This is clearly different from the definition of the experimental value which is defined as the yield stress at 0.2% plastic strain. In the present work, to be consistent with the definition of the yield stress, loading and unloading simulations were performed. The maximum total strain during the loading was adjusted so as to obtain a 0.2% residual *plastic* strain at zero stress level.

The maximum stress during loading represents the yield stress, see Fig. 5. Note that for large grain size, the unloading response is clearly elastic, while for small grain size (10 nm on Fig.5), the material behaves like a viscoelastic one, indicating a change in the deformation mode. This change will be associated with the extinction of the dislocation glide contribution for small grain size.

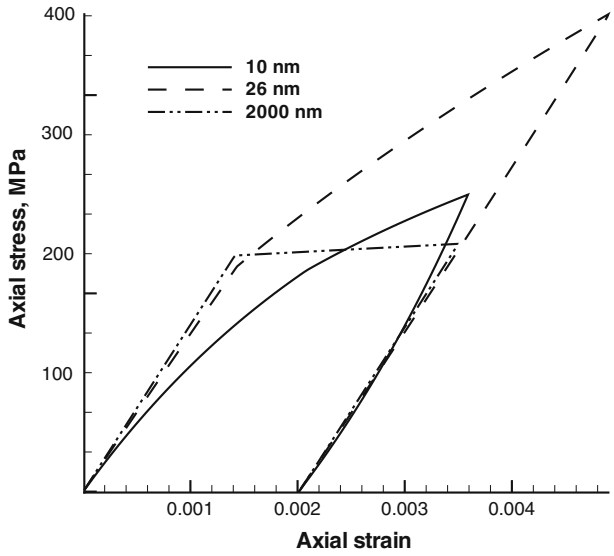

Fig. 5 Tensile loading and unloading for different grain sizes. The macroscopic strain-rate tensor corresponds to uniaxial tension: $D_o = 10^{-3}$ s^{-1} for loading and $D_o = -10^{-3}$ s^{-1} for unloading. The maximum total strain is adjusted for each material so as to obtain a 0.2% residual strain at zero stress level. The maximum stress represents the yield stress $\sigma_{0.2\%}$ at 0.2% offset

The evolution of the yield stress versus $d^{-1/2}$ is presented on Fig. 6. As before, macroscopic loading corresponds to uniaxial tension with $D_o = 10^{-3}\,\mathrm{s}^{-1}$. Clearly, both the Hall–Petch and the inverse Hall–Petch type behaviors are present. For average grain size over 20 nm, the flow stress increases with grain refinement. Below 20 nm, the reverse trend is observed. The results were obtained with the parameter values presented in Table 1. On this figure, yield stresses measured by [27] are shown for validation. A fairly good agreement is seen. A better fit can be obtained by modifying some parameters, *viz*. with $\sigma_o = 250$ MPa and $D^{sd}_{GB} = 5 \cdot 10^{-20}$m^2/s. In the literature, a great deal of data on the grain size dependence of stress in nanocrystalline Cu are available, cf. the compilations in [1, 26, 32, 33]. However, these data are too diverse to be suitable for a comparison with a particular model calculation. Not only do they refer to materials of different provenience, but they often correspond to various strains and strain rates and are not always representative of the yield stress. Most of the compilations refer to the pioneering work by Sanders et al. [27], but in many cases, e.g. [32], the yield stresses recalculated from the hardness data are quoted. It was shown in [27] that the latter are higher than the true yield stresses obtained directly from

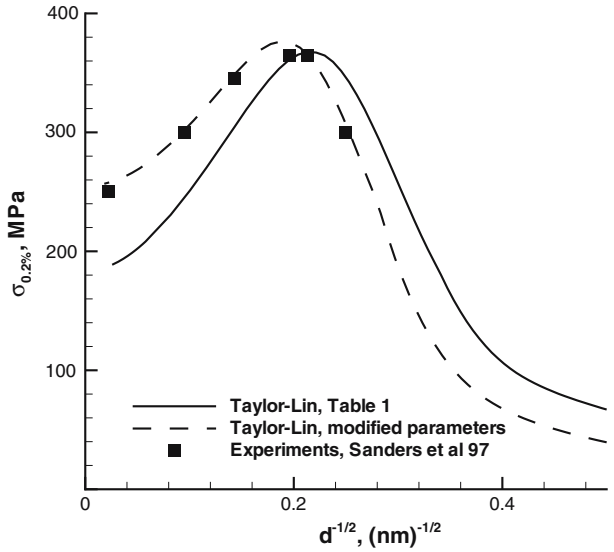

Fig. 6 Hall–Petch behavior of nanocrystalline copper. The macroscopic strain rate tensor corresponds to uniaxial tension with $D_o = 10^{-3}$ s^{-1}. The yield stress is defined as the stress for a residual strain of 0.2% and is calculated as illustrated in Fig. 5. A fairly good agreement with the experiments of Sanders et al. [27] is obtained. The material parameters available in the literature are summarised in Table 1. A better fit is proposed for a different set of parameters: $\sigma_o = 250$ MPa and $D_{GB}^{sd} = 5 \cdot 10^{-20}$m^2/s

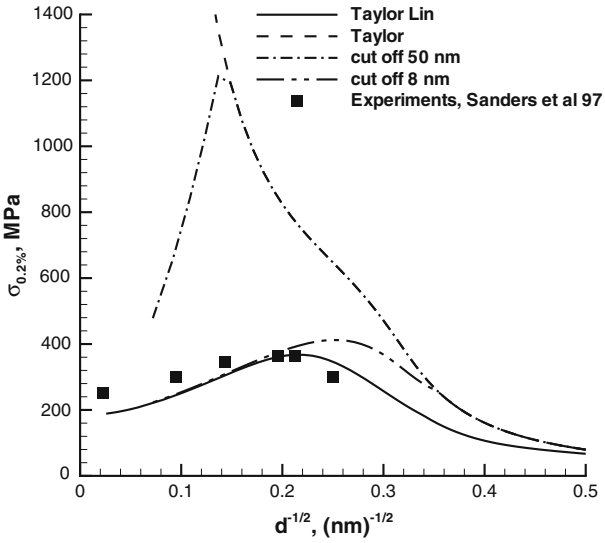

Fig. 7 Predictions of the yield stress $\sigma_{0.2}$ obtained using the Taylor–Lin and the Taylor approaches. With the Taylor approach, the introduction of a saturation of the flow stress of the grain boundary phase is necessary to reproduce experimental data. The Taylor–Lin approach that includes elasticity is able to predict the experiments correctly, without any extra assumptions

stress–strain curves. We therefore used the original yield stress data from [27] as a basis for validation of the model predictions. Other models available in the literature are able to predict the inverse Hall–Petch behavior for nanomaterials. For example, the work of Jiang and Weng [10] can be mentioned. With a generalized self-consistent approach and specific behaviors of the grain interior and grain boundary phases, they obtained results also in close agreement with [27], see Fig. 5 of [10]. However, the same cut-off value as in [2] was adopted in [10] for the plastic behavior of the grain interior phase. In our approach, no cut-off parameter is necessary to reproduce the measured yield stresses with good accuracy.

Figure 7 compares the Taylor–Lin approach with a Taylor scheme (no elasticity). For large grain size, the yield stress reaches unrealistically high values. Under a rigid Taylor scheme, the viscoplastic strain rate is equal to the macroscopic strain rate. For large grain size ($f \approx 1$), the diffusion activity in the crystallite almost disappears and thus $\underline{d}_{GI}^{disl} = \underline{D}$. As a consequence the term $f\underline{s}_{GI}$ in Eq. 14 is scaled by $\sigma_o(D^{eq}/D^*)^m$ which is naturally bound. The origin of the high flow stress level is due to the grain boundary behavior described by Eqs. 4 and 5. It can be easily proved that, for large grain material, the term $(1-f)\underline{s}_{GB}$ is proportional to the grain size d. As a consequence, to obtain realistic prediction using rigid Taylor scheme, a saturation of the grain boundary flow stress is needed. As already mentioned, [2] used such a saturation assumption, see Figs. 8 and 9 of their article. In that spirit, to saturate the GB flow stress level (used only for the rigid Taylor scheme), the term d in Eq. 4 is replaced by $d = \inf(d,d_c)$, d_c representing a cut-off value. Two

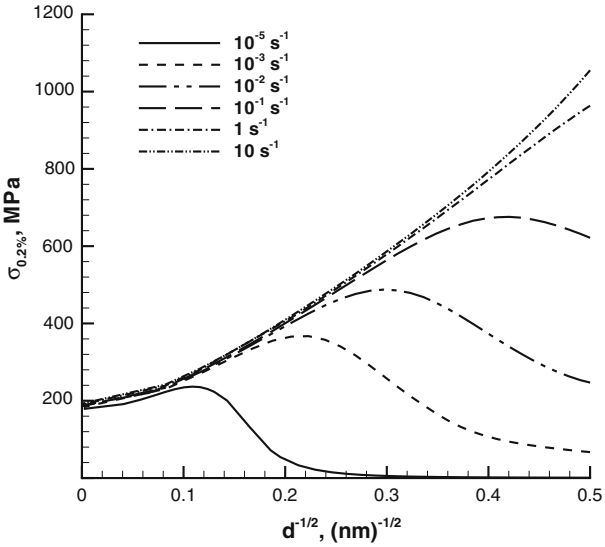

Fig. 8 Evolution of the yield stress for different macroscopic loading rates. The transition point from a Hall–Petch regime to an inverse Hall-Petch trend moves towards smaller grain sizes as strain rate increases

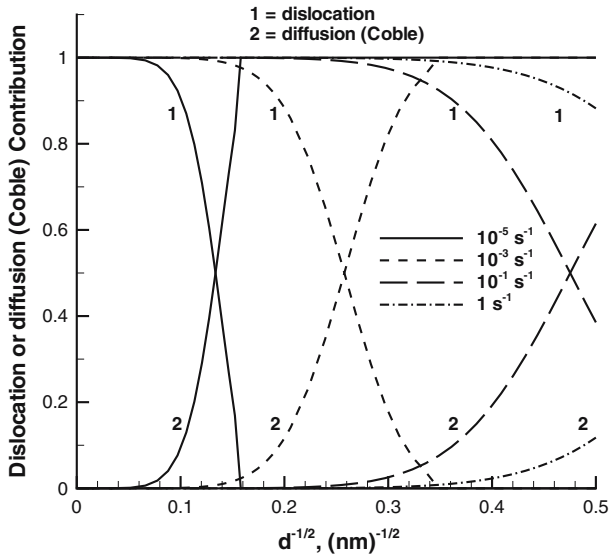

Fig. 9 Variation of the relative contribution of the dislocation glide and diffusion (mainly Coble creep) in the crystallite. Macroscopic strain rate is varied from 10^{-5} s^{-1} to 1 s^{-1}. For high strain rates and/or for large grain sizes, dislocation glide is the predominant plastic deformation mode in the crystallite

different values of d_c were tested and the corresponding predictions are presented in Fig. 7. For a reasonable choice of $d_c = 8\,\text{nm}$ and with $D_o = 10^{-3}\,s^{-1}$, [2], the viscoplastic Taylor scheme (without elasticity) appears to give realistic predictions. However, the present Taylor-Lin homogenisation scheme is preferable as it does not require the use of such cut-off parameters.

The effect of the loading rate is investigated in Fig. 8. As the strain rate increases, the transition from a Hall–Petch to an inverse Hall–Petch trend moves to smaller grain sizes. To explain this effect, it is important to identify the relative contributions of dislocation glide and diffusion to the plastic deformation of the crystallite, see Fig. 9. From numerical simulations, it appears that the Nabarro–Herring creep has almost no influence on the deformation of the crystallite, so that the prevalent diffusion-controlled mechanism in the crystallite is the Coble creep. As the strain rate increases, the dislocation glide mechanism remains active also for small grain size. Coble creep and dislocation glide are acting in parallel. The same stress σ_{GI}^{eq} operates for each deformation mechanism. From Eqs. 8 and 12, one obtains:

$$\sigma_{GI}^{eq} = \frac{kTd^3}{14\pi\Omega_b w D_{bd}^{sd}} d_{GI}^{Co-eq} = \sigma_o \left(\frac{d_{GI}^{disl-eq}}{d_*}\right)^{\frac{1}{m}} \sqrt{\frac{\rho}{\rho_o}} \qquad (18)$$

For a given grain size, as the macroscopic strain rate increases, the stress level in the crystallite increases only slightly, as m is large and ρ does not evolve strongly for low strain. Therefore, the strain rate d_{GI}^{Co-eq} associated with the Coble creep is almost unchanged. Due to the increase of the total strain rate, the total plastic strain rate inside the crystallite increases as well, so that the dislocation contribution is enhanced, see Fig. 9. With similar arguments, for a given total strain rate, as the grain size increases, the level of the flow stress σ_{GI}^{eq} will not change strongly. From the expression for the Coble creep, Eq. 18, it is seen that $d_{GI}^{Co\text{-}eq}$ decreases and thus the contribution of $d_{GI}^{disl\text{-}eq}$ must increase. To summarize, for high strain rates and/or large grain sizes, dislocation glide is the major mechanism for the plastic deformation of the crystallite, see Fig. 9. The change in dominant plastic deformation mechanism in the crystallite leads to the transition from a Hall–Petch to an inverse Hall–Petch behavior. From Fig. 8, the grain size d_{tr} corresponding to the transition decreases from 85 nm at 10^{-5} s^{-1} to 6 nm at 0.1 s^{-1}. For strain rate larger than 1 s^{-1}, no inverse Hall–Petch trend is predicted. An approximate relationship between d_{tr} and D_o is derived in Appendix A:

$$d_{tr}^7 D_o^2 = \text{const} \qquad (19)$$

Figure 10 shows a close agreement between the d_{tr} values obtained with the proposed model and with Eq. 19. Note that the value of the constant on the right-

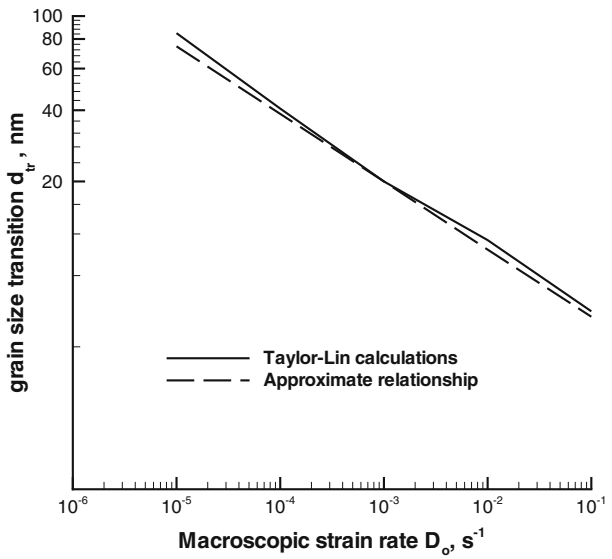

Fig. 10 Variation of the transition grain size d_{tr} with the macroscopic strain rate. The transition grain size separating the Hall–Petch from the inverse Hall–Petch regime decreases with increasing strain rate. The relation $D_o^2 d_{tr}^7 = \text{const}$ derived in Appendix A appears to be a good approximation compared to predictions with the Taylor–Lin model

hand side of Eq. 19 has been identified considering that $d_{tr} = 20$ nm at $D_o = 10^{-3}\,s^{-1}$.

Finally, the variation of the global strain rate sensitivity defined as $\left(\frac{\partial \log S^{eq}}{\partial \log D^{eq}}\right)_{\varepsilon}$ is considered for different grain sizes. The strain rate sensitivity is calculated for a given total strain $\varepsilon = 0.01$. As already mentioned, for large strain rate or large grain size the predominant plastic deformation mechanism in the crystallite is dislocation glide. The attendant strain rate sensitivity of the flow stress is close to 1/230, see zoom in Fig. 11. For low loading rates and/or small grain sizes, the diffusion-controlled mechanism (Coble creep) is predominant. Thus, the corresponding strain rate sensitivity increases. These results are in keeping with those obtained by [3] using the Taylor approach (without elasticity). From experiments, macroscopic strain rate sensitivities were evaluated from tensile stress–strain curves at different loading rates. An increase of the strain rate sensitivity of the flow stress for nanocrystalline materials as compared with that for coarse grained materials was also observed experimentally, cf. [26]. In their work, the authors observed that the nanocrystalline material with an average grain size of 62 nm had a strain rate sensitivity of 0.027, whereas for coarse-grained copper, the strain rate sensitivity was 0.006. A similar effect of the grain size on the strain rate sensitivity of the flow stress of Al was observed by [34], see also [1]. Values close to unity expected from the present model for very small grain sizes and low strain rates have never been observed, which means that further improvements of modelling are still needed. The role of diffusion-controlled mechanisms, which in the limit of very small grain size should yield a strain-rate sensitivity tending to unity, appears to have been overestimated in the present modelling.

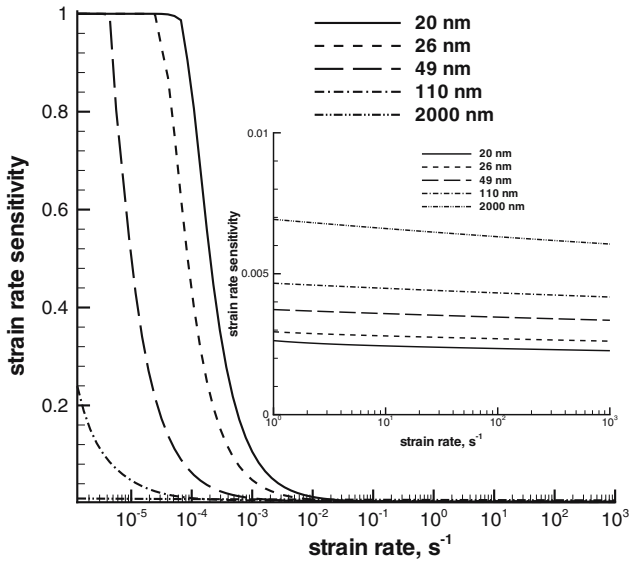

Fig. 11 Strain rate sensitivity of the flow stress at 1% total strain as a function of the macroscopic strain rate D_o. The dependence is presented for different grain sizes, from the nanometer up to the micrometer range. For large strain rates, the dislocation glide is prevalent, so that low values of the strain rate sentivity are observed. As the strain rate decreases, the contribution of the diffusion-controlled mechanism increases, and so does the strain rate sensitivity

Conclusion

An extension of models proposed by Kim et al. [2] and Kim and Estrin [3] has been presented. The major contribution of the present study consists in the introduction of elasticity in the material description. With elasticity, the yield stress can be evaluated with better accuracy. A comparison with experiments of Sanders et al. [27] yields a fairly good agreement. The transition from a Hall–Petch regime to an inverse trend has been explained by the change in plastic deformation mode in the crystallite phase from a dislocation glide driven mechanism to a diffusion-controlled process. A relation between transition grain size and macroscopic strain rate has been derived. The present approach seems to be reasonable for estimating macroscopic mechanical behavior and the related properties at small strain. Improvements need to be made to provide a physically based model for large strain as well.

Acknowledgements The authors would like to thank Prof. Hyoung Seop Kim (Chungnam National University, Daejeon, KOREA) for useful discussions

Appendix A: Relation between the transition grain size d_{tr} and loading rate D_o

The transition from the Hall–Petch to an inverse Hall–Petch behavior with a decrease in the grain size is due to a change in the plastic deformation mechanism in the crystallite phase, see Figs. 8 and 9. For coarse grained materials, dislocation glide is predominant, while for fine grained ones, diffusion-controlled Coble creep is the main deformation mechanism. Based on Figs. 8 and 9, one can postulate that the transition occurs when the two modes of deformation contribute almost equally to the total viscoplastic strain rate of the crystallite. Thus the transition occurs when the following condition is fulfilled:

$$d_{GI}^{disl-eq} = d_{GI}^{Co-eq} \tag{20}$$

From relation (18), the dislocation strain rate $d_{GI}^{disl-eq}$ can be linked to the Coble creep rate d_{GI}^{Co-eq}.

Then using relation (20), the equivalent total plastic strain rate $d_{\mathrm{GI}}^{\mathrm{vp-eq}}$, as defined by Eq. 7 is expressed (neglecting the Nabarro-Herring creep contribution) as a function of the Coble creep strain rate $d_{\mathrm{GI}}^{\mathrm{Co-eq}}$:

$$d_{\mathrm{GI}}^{\mathrm{vp-eq}} = 2d_* \left(\frac{kTd_{\mathrm{tr}}^3}{14\pi\Omega_b D_{\mathrm{bd}}^{\mathrm{sd}} w\sigma_{\mathrm{o}}} d_{\mathrm{GI}}^{\mathrm{Co-eq}} \right)^m \left(\frac{\rho}{\rho_{\mathrm{o}}} \right)^{-\frac{m}{2}} \tag{21}$$

Here, d_{tr} is the transition grain size for which relation (20) is satisfied. Due to elasticity, the total plastic strain rate in the crystallite is lower than the total macroscopic strain rate D_{o}. A scalar β is introduced so that:

$$d_{\mathrm{GI}}^{\mathrm{vp-eq}} = \beta D_{\mathrm{o}} \tag{22}$$

The last term to be evaluated is ρ/ρ_{o}. Considering that the dominant term for small strain in Eq. 7 is related to the constant C and that C is large for a nanocrystalline material, the dislocation density is approximately proportional to the inverse of the grain size d_{tr}:

$$\frac{\rho}{\rho_{\mathrm{o}}} = \frac{K}{d_{\mathrm{tr}}} \tag{23}$$

Therefore, combining Eqs 22 and 23, one obtains the following relation between D_{o} and d_{tr}:

$$\beta \frac{D_{\mathrm{o}}}{2} = d^* \left(\frac{kTd_{\mathrm{tr}}^3}{28\pi\Omega_b D_{\mathrm{bd}}^{\mathrm{sd}} w\sigma_{\mathrm{o}}} \beta D_{\mathrm{o}} \right)^m \left(\frac{K}{d_{\mathrm{tr}}} \right)^{-\frac{m}{2}} \tag{24}$$

Since m is much larger than unity, this equation leads to:

$$(\beta D_{\mathrm{o}})^2 = \left(\frac{28\pi\Omega_b D_{\mathrm{bd}}^{\mathrm{sd}} w\sigma_{\mathrm{o}}}{kTd_{\mathrm{tr}}^3} \right)^2 \frac{K}{d_{\mathrm{tr}}} \tag{25}$$

Finally, assuming that β and K will not vary strongly with loading conditions, one obtains:

$$D_{\mathrm{o}}^2 d_{\mathrm{tr}}^7 = \mathrm{const} \tag{26}$$

Appendix B: Relationship between equivalent stresses

During uniaxial tensile loading, the material is subjected to the following macroscopic stress:

$$\underline{\Sigma} = \begin{bmatrix} \Sigma_{11} & 0 & 0 \\ 0 & 0 & 0 \\ 0 & 0 & 0 \end{bmatrix} \tag{27}$$

In the present work, the material is assumed isotropic. Since the loading is axisymetric and due to the Taylor–Lin assumption for which the local strain rate in each phase is equal to the macroscopic strain rate, the stress state in the grain interior can be written as:

$$\underline{\sigma}_{\mathrm{GI}} = \begin{bmatrix} \sigma_{11}^{\mathrm{GI}} & 0 & 0 \\ 0 & \sigma_{22}^{\mathrm{GI}} & 0 \\ 0 & 0 & \sigma_{22}^{\mathrm{GI}} \end{bmatrix} \tag{28}$$

The stress state in the grain boundary is given by Eq. 28 replacing the superscript GI by GB. With volume averaging, the macroscopic stress $\underline{\Sigma}$ is linked to stresses $\underline{\sigma}_{\mathrm{GI}}$ and $\underline{\sigma}_{\mathrm{GB}}$ in the two phases by:

$$\underline{\Sigma} = f\underline{\sigma}_{\mathrm{GI}} + (1-f)\underline{\sigma}_{\mathrm{GB}} \tag{29}$$

Here, f represents the volume fraction of the grain interior. By combination of Eqs. 28 and 29, one obtains:

$$\Sigma_{11} = f\sigma_{11}^{\mathrm{GI}} + (1-f)\sigma_{11}^{\mathrm{GB}}, \quad f\sigma_{22}^{\mathrm{GI}} + (1-f)\sigma_{22}^{\mathrm{GB}} = 0 \tag{30}$$

The grain interior and grain boundary phases are not subjected to uniaxial tensile loading. Nevertheless, the volume average of the microscopic stresses restitutes a stress tensor of uniaxial tension.

The deviatoric Cauchy stress tensor in the grain interior $\underline{s}_{\mathrm{GI}}$, obtained from relation (28) is given by:

$$\underline{s}_{\mathrm{GI}} = \begin{bmatrix} \frac{2}{3}\sigma_{\mathrm{GI}}^{\mathrm{eq}} & 0 & 0 \\ 0 & -\frac{1}{3}\sigma_{\mathrm{GI}}^{\mathrm{eq}} & 0 \\ 0 & 0 & -\frac{1}{3}\sigma_{\mathrm{GI}}^{\mathrm{eq}} \end{bmatrix} \tag{31}$$

with $\sigma_{\mathrm{GI}}^{\mathrm{eq}} = \sigma_{11}^{\mathrm{GI}} - \sigma_{22}^{\mathrm{GI}}$ being the equivalent stress in the grain interior phase. The same expression is valid for $\underline{s}_{\mathrm{GB}}$ with replacing GI by GB in expression (31). Using Eq. 14, the macroscopic deviatoric Cauchy stress components are:

$$S_{11} = \frac{2}{3}(f\sigma_{\mathrm{GI}}^{\mathrm{eq}} + (1-f)\sigma_{\mathrm{GB}}^{\mathrm{eq}}) \quad S_{22} = -\frac{S_{11}}{2} \quad S_{33} = -\frac{S_{11}}{2} \tag{32}$$

The equivalent macroscopic stress Σ^{eq} has the form:

$$\Sigma^{eq} = f\sigma_{GI}^{eq} + (1-f)\sigma_{GB}^{eq} \quad (33)$$

References

1. Meyers MA, Mishra A, Benson DJ (2006) Prog Mater Sci 51:427
2. Kim HS, Estrin Y, Bush MB (2000) Acta Mater 48:493
3. Kim HS, Estrin Y (2005) Acta Mater 53:765
4. Carsley JE, Ning J, Milligan WW, Hackney SA, Aifantis EC (1995) Nanostruct Mater 5:441
5. Konstantinidis DA, Aifantis EC (1998) Nanostruct Mater 10:1111
6. Gutkin MYu, Ovid'ko IA, Pande CS (2001) Rev Adv Mater Sci 2:80
7. Estrin Y, Kim HS, Bush MB (2004) In: Nalwa HS (ed) Encyclopedia of nanoscience and nanotechnology, vol. 8. American Scientific Publishers, p 489
8. Capolungo L, Jochum C, Cherkaoui M, Qu J (2004) Int J Plasticity 21:67
9. Capolungo L, Cherkaoui M, Qu J (2005) J Eng Mater Techn 127:400
10. Jiang B, Weng GJ (2004) J Mech Phys Solids 52:1125
11. Christensen RM, Lo KH (1979) J Mech Phys Solids 27:315
12. Luo HA, Weng GJ (1987) Mech Mater 6:347
13. Lin TH (1957) J Mech Phys Solids 5:143
14. Mori T, Tanaka K (1973) Acta Metall 21:571
15. Molinari A (2002) J Engng Mater Technol 124:62
16. Taylor GI (1983) J Inst Metals 62:307
17. Asaro RJ, Needleman A (1985) Acta Metall 33:923
18. Bronkhorst CA, Kalidindi SR, Anand L (1992) Phil Trans Roy Soc London A 341:443
19. Zouhal N, Molinari A, Tóth LS (1996) Int J Plasticity 12:343
20. Tóth LS, Molinari A, Zouhal N (2000) Mech Mat 32:99
21. Saanouni K, Abdul-Latif A (1996) Int J Plasticity 12:1111
22. Abdul-Latif A, Saanouni K (1996) Int J Plasticity 12:1123
23. Zhu B, Asaro RJ, Krysl P, Bailey R (2005) Acta Mater 53:4825
24. Jia D, Ramesh KT, Ma E (2003) Acta Mater 51:3495
25. Estrin Y (1996) In: Krausz AS, Krausz K (eds) Unified contitutive laws of plastic deformation. Academic Press, New-York, p 489
26. Cheng S, Ma E, Wang YM, Kecskes LJ, Youssef KM, Koch CC, Trociewitz UP, Han K (2005) Acta Mater 53:1521
27. Sanders PG, Eastman JA, Weertman JR (1997) Acta Mater 45:4019
28. Chokshi AH, Rosen A, Karch J, Gleiter H (1989) Scr Metall 23:1679
29. Van Swygenhoven H, Weertman J (2003) Scripta Mater 49:625
30. Fu HH, Benson DJ, Meyers MA (2001) Acta Mater 49:2567
31. Fu HH, Benson DJ, Meyers MA (2004) Acta Mater 52:4413
32. Masumura RA, Hazzledine PM, Pande CS (1998) Acta mater 46:4527
33. Conrad H (2003) Mater Sci Eng A 341:216
34. May J, Höppel HW, Göken M (2005) Scripta Mater 53:189